

(Pro)renin receptor signaling in hypothalamic tyrosine hydroxylase neurons is required for obesity-associated glucose metabolic impairment

Shiyue Pan,^{1,2} Lucas A.C. Souza,^{1,2} Caleb J. Worker,^{1,2} Miriam E. Reyes Mendez,^{1,2} Ariana Julia B. Gayban,^{1,2} Silvana G. Cooper,^{1,2} Alfredo Sanchez Solano,^{1,2} Richard N. Bergman,³ Darko Stefanovski,⁴ Gregory J. Morton,⁵ Michael W. Schwartz,⁵ and Yumei Feng Earley^{1,2}

¹Departments of Pharmacology and Physiology & Cell Biology and ²Center for Molecular and Cellular Signaling in the Cardiovascular System, University of Nevada, Reno, Reno, Nevada, USA. ³Diabetes and Obesity Research Institute, Cedars-Sinai Medical Center, Los Angeles, California, USA. ⁴New Bolton Center, School of Veterinary Medicine, University of Pennsylvania Philadelphia, Pennsylvania, USA. ⁵University of Washington Medicine Diabetes Institute, University of Washington, Seattle, Washington, USA.

Glucose homeostasis is achieved via complex interactions between the endocrine pancreas and other peripheral tissues and glucoregulatory neurocircuits in the brain that remain incompletely defined. Within the brain, neurons in the hypothalamus appear to play a particularly important role. Consistent with this notion, we report evidence that (pro)renin receptor (PRR) signaling within a subset of tyrosine hydroxylase (TH) neurons located in the hypothalamic paraventricular nucleus (PVNTH neurons) is a physiological determinant of the defended blood glucose level. Specifically, we demonstrate that PRR deletion from PVNTH neurons restores normal glucose homeostasis in mice with diet-induced obesity (DIO). Conversely, chemogenetic inhibition of PVNTH neurons mimics the deleterious effect of DIO on glucose. Combined with our finding that PRR activation inhibits PVNTH neurons, these findings suggest that, in mice, (a) PVNTH neurons play a physiological role in glucose homeostasis, (b) PRR activation impairs glucose homeostasis by inhibiting these neurons, and (c) this mechanism plays a causal role in obesity-associated metabolic impairment.

Introduction

The term “glucose homeostasis” refers to a complex set of coordinated responses that collectively maintain the circulating glucose level within narrow limits by balancing glucose entry into and removal from the bloodstream over time. While the pancreas and liver are vital to this process, growing evidence implicates a key role for the CNS, with the hypothalamus playing a particularly important role (1–3). Experimental activation of a subset of neurons in the hypothalamic ventromedial nucleus (VMN), for example, potently increases the blood glucose level (4), whereas inactivation of this subset both impairs glucose counterregulation and blunts hyperglycemia induced by streptozotocin (5). Moreover, the activity of these neurons decreases rapidly following an increase in the blood glucose level, suggesting that, like pancreatic β cells, these neurons are capable of detecting and responding to changes in glycemia (6).

Another hypothalamic area implicated in glucose homeostasis is the paraventricular nucleus (PVN). Like the VMN, this brain area plays a key role in autonomic regulation, and contained within it are several distinct neuronal subpopulations that have been shown to influence circulating levels of insulin, glucose, or both (7–9). Among these is a subset of PVN neurons marked by expression of tyrosine hydroxylase (TH) (PVNTH neurons) (10) that have been implicated in fuel homeostasis (11). In the current work, we hypothesized that these neurons, like neurons in the VMN, participate in autonomic control of glucose homeostasis. The current studies were undertaken to investigate this hypothesis.

Best known for its role in controlling blood pressure and cardiovascular function, the renin-angiotensin system (RAS) is also implicated in the control of glucose homeostasis. For example, excessive RAS activity is associated with obesity and insulin resistance in humans (12, 13), and it has been suggested to play

Conflict of interest: The authors have declared that no conflict of interest exists.

Authorship note: SP, LACS, CJW, MERM, and AJBG contributed equally to this work and are co-first authors.

Copyright: © 2024, Pan et al. This is an open access article published under the terms of the Creative Commons Attribution 4.0 International License.

Submitted: September 1, 2023

Accepted: February 8, 2024

Published: February 13, 2024

Reference information: *JCI Insight*. 2024;9(6):e174294.
<https://doi.org/10.1172/jci.insight.174294>.

a causal role in obesity-associated metabolic impairment (14, 15). One potential mechanism that might contribute to these effects is excessive RAS activity in the brain, which can mediate deleterious effects by activating neuronal (pro)renin receptors (PRRs) (16, 17). Upon binding to either of its ligands (prorenin or renin) (18–20), the PRR generates angiotensin II (Ang II) while also functioning as a tyrosine kinase that can engage multiple intracellular signal transduction cascades. Interestingly, whereas renin circulates at normal or low levels in patients with obesity and diabetes (21–23), plasma levels of prorenin are elevated in this population (23–28); in a mouse model of diet-induced obesity (DIO), prorenin levels are elevated in the hypothalamus as well as in plasma (29). Moreover, targeted deletion of neuronal PRR was recently shown to ameliorate glucose metabolic impairment in these animals (29).

The goal of the current work is to identify neuronal subsets upon which PRR signaling acts to impair glucose homeostasis. Based on our finding that the vast majority of PVNTH neurons express the PRR, we focused on the specific question of whether PRR activity in these neurons is linked to obesity-associated metabolic impairment. We report that (a) the PRR is expressed by a large percentage of PVNTH neurons, (b) PRR activation potently inhibits these neurons, (c) chemogenetic inhibition of PVNTH neurons mimics the effect of a high-fat diet (HFD) to impair glucose homeostasis, and (d) selective deletion of the PRR from these neurons ameliorates the effect of DIO on both the circulating glucose level and glucose tolerance. Since these effects occurred in the absence of significant differences in body weight, our data suggest that, in normal animals, PVNTH neurons play a physiological role in promoting normal glucose homeostasis — independently of the control of body weight — and that inhibition of these neurons by increased PRR signaling contributes to the effect of obesity to impair glucose homeostasis.

Results

Expression of the PRR and vasopressin by PVNTH neurons in mice. *Prr* mRNA and PRR protein are expressed by neurons in both the rodent and human brain (30, 31), including presympathetic and vasopressin-containing neurons in the PVN (32, 33). To determine if either PRR or vasopressin are expressed in PVNTH neurons, we used RNAScope in situ hybridization. Negative controls detecting the bacterial gene *DapB* were included to exclude nonspecific/background staining (Supplemental Figure 1; supplemental material available online with this article; <https://doi.org/10.1172/jci.insight.174294DS1>). We report that, in the PVN, the vast majority of *Th* mRNA expression is colocalized with *Prr* mRNA (Figure 1, A–D). Thus, quantitative analysis of 1,807 TH neurons throughout the PVN (bregma, –0.58 mm to –1.06 mm) revealed that approximately 95% of the PVNTH neurons express the *Prr* mRNA (Figure 1E). By comparison, only 56% of *Prr*-expressing neurons coexpress *Th* mRNA (Figure 1F). We also report that only 19% of 1,433 TH⁺ PVN neurons coexpress vasopressin (bregma, –0.58 mm to –1.06 mm) (Figure 1, G–K), although 60% of vasopressin⁺ neurons in this brain area coexpress *Th* mRNA (Figure 1L).

Validation of PRR deletion from PVNTH neurons. Having established that most PVNTH neurons express PRR, we next sought to investigate the role played by PRR signaling by deleting the PRR specifically from PVNTH neurons. This goal was achieved by bilateral microinjection of a viral vector that expresses cre recombinase under the control of the rat TH promoter (AAV2-rTH-Cre) into the PVN. To enable visualization of virally mediated recombination in TH-expressing neurons, double-floxed mice in which both the PRR allele and a STOP cassette for tdTomato are flanked by loxP sites (PRR-tdTomato-LoxP) and their controls (loxP-flanked-STOP tdTomato allele only; tdTomato-LoxP; Control) were studied (Figure 2A). Following the microinjection of AAV2-rTH-Cre into the PVN of these mice, tdTomato expression was induced specifically in TH-expressing neurons (Figure 2B, left panel), and PRR deletion from these neurons (PVNTH-PRRKO) was confirmed 1 month after microinjection by immunofluorescence labeling (Figure 2, B and C). These data indicate that PRR deletion was successful in just half of PVNTH neurons. We anticipate that, in future studies, the phenotype induced by PVNTH neuron-specific KO will be more robust if achieved in a larger fraction of these neurons.

Effect of selective deletion of PRR from PVNTH neurons on glucose homeostasis. Using this approach (also illustrated in Figure 3A), PVNTH-PRRKO and their controls were allowed 4 weeks to recover from and to allow for viral expression after adeno-associated virus (AAV) microinjection. Mice were then placed on either an HFD (60% Kcal from fat) or a matched, low-fat control diet (LFD) (10% Kcal from fat) for the next 6 weeks (Figure 3B). Male and female mice were studied separately.

In males, deletion of PRR in PVNTH neurons in the LFD-fed group (LFD-PVNTH-PRRKO) had no significant effect on either body weight (Figure 3C) or fasting blood glucose (FBG) (Figure 3E), although

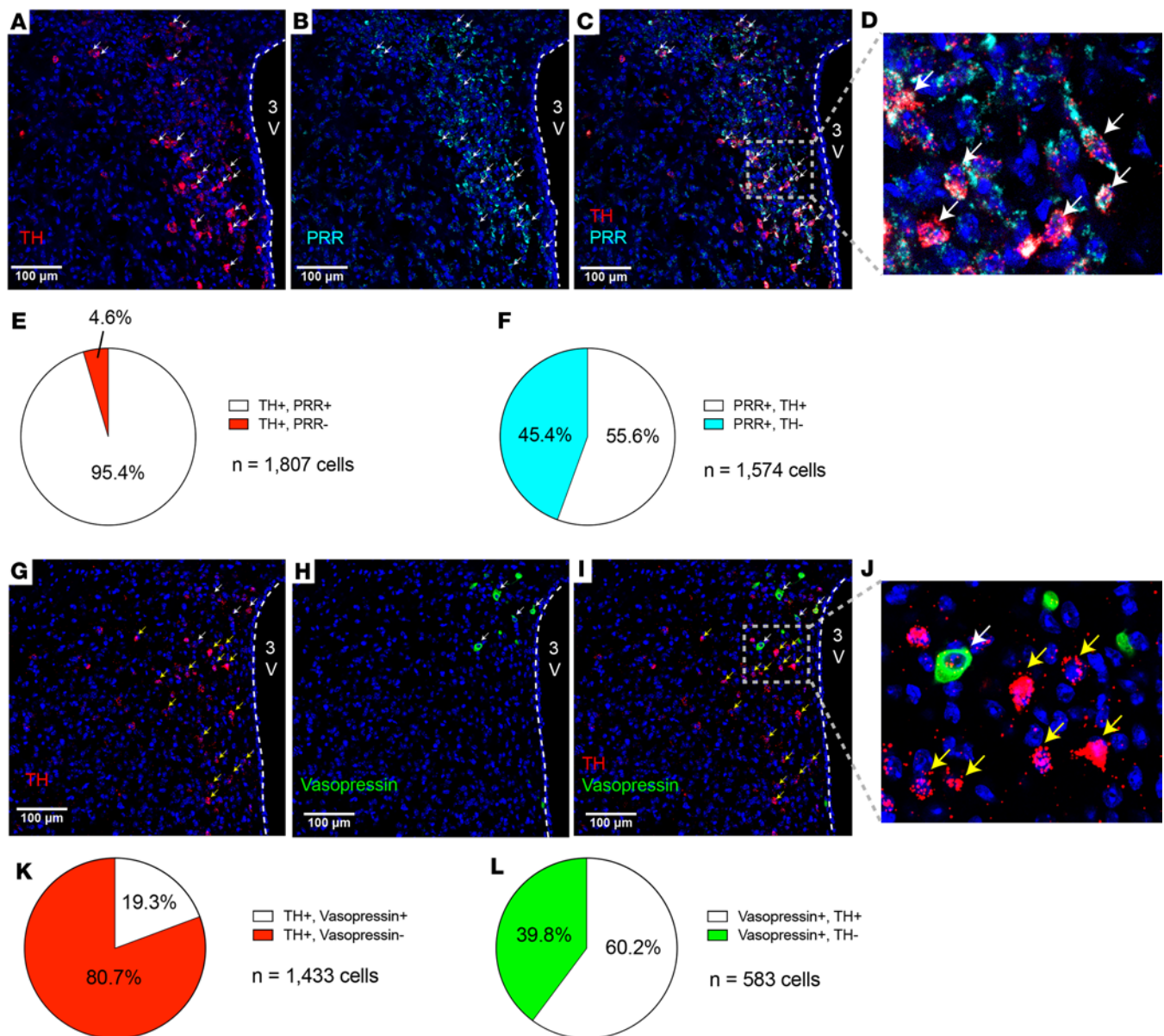


Figure 1. Expression of (pro)renin receptor and vasopressin in the PVNTH neurons. (A and B) Representative images of RNAScope in situ hybridization of Th (red), Prr (cyan), and DAPI (blue) in the mouse PVN (bregma, -0.82 mm). (C) Merged image showing colocalization of Th and Prr mRNA in the PVN. (D) Digital enlarged views of the gray boxed areas in C. White arrows indicate cells expressed both Th and Prr mRNA. (E and F) Quantification of Th and Prr colocalization in the PVN ($n = 6$ mice; E, $n = 3$ mice; F). (G and H) Representative images of RNAScope in situ hybridization of Th (red), vasopressin (green), and DAPI (blue) in the mouse PVN (bregma, -0.88 mm). (I) Merged image showing colocalization of Th and vasopressin mRNA in the PVN. (J) Digital enlarged views of the gray boxed areas in I. White arrows indicate cells expressed both Th and vasopressin mRNA. Yellow arrows indicate cells expressed Th mRNA without vasopressin mRNA. (K and L) Quantification of TH and vasopressin colocalization in the PVN ($n = 3$ mice). PVN slices from bregma -0.58 mm to -1.06 mm were used. Scale bars: 100 μ m.

calorie intake was slightly reduced (Figure 3D) relative to LFD-Control. As expected, the 6-week HFD regimen increased body weight (Figure 3C), calorie intake (Figure 3D), and FBG levels (Figure 3E) in controls (HFD-Control) compared with their LFD-fed counterparts (LFD-Control). Despite similar increases in body weight (Figure 3C), FBG levels were significantly lower in HFD-PVNTH-PRRKO mice than in HFD-control mice (Figure 3E).

To confirm these findings and to detect any background- or strain-dependent effects of PVNTH-PRRKO, we performed a complementary study in a strain of male mice bearing the floxed PRR allele but without the floxed tdTomato reporter (PRR^{fl/y} mice). Following bilateral microinjection into the PVN of either a control virus (AAV2-TH-GFP) or AAV2-rTH-Cre to delete PRR in PVNTH neurons into male

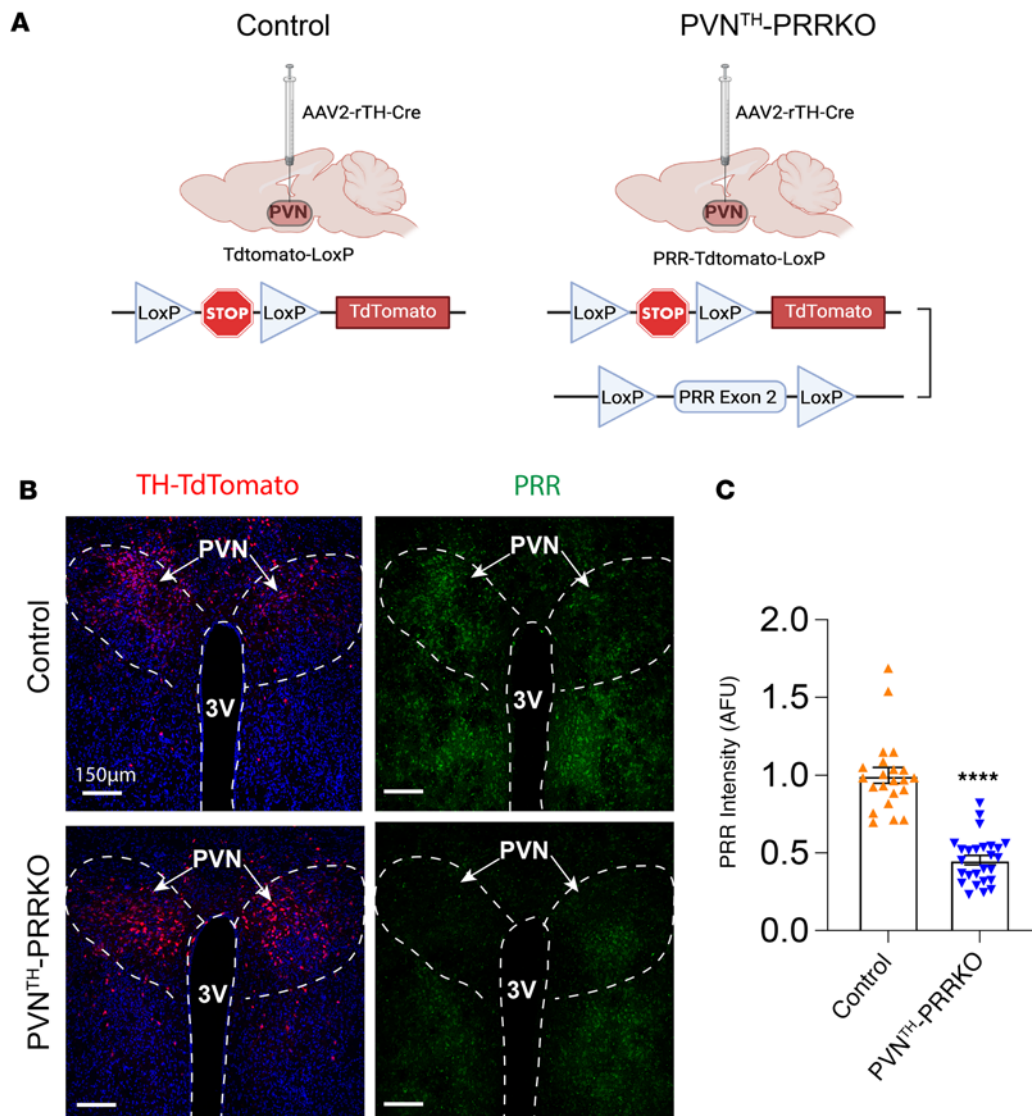


Figure 2. Validation of (pro)renin receptor (PRR) knockdown efficiency in PVNTH neurons. (A) Schematic representation of Cre-LoxP-mediated deletion of PRR in PVNTH neurons in tdTomato-LoxP (tdTomato^{fl/fl}) or PRR-tdTomato-LoxP mice. AAV-expressing Cre recombinase driven by a rat tyrosine hydroxylase promoter (AAV2-rTH-Cre) was used to delete PRR and induce tdTomato reporter expression in mice bearing both PRR-LoxP and tdTomato-LoxP alleles, shown as PVNTH-PRRKO. The tdTomato-LoxP mice received the AAV2-rTH-Cre to the PVN and were used as a control. (B) Representative images showing TH-TdTomato (red), DAPI (blue), and PRR immunofluorescence (green) in the PVN (bregma, -1.06 mm). Scale bar: 150 μ m. (C) Quantification data of PRR immunoreactive intensity. Data are expressed as mean \pm SEM. *****P* < 0.0001, unpaired Student's *t* test. (*n* = 3 animals/group, 22–26 PVNs/group).

PRR^{fl/y} mice (Supplemental Figure 2A), animals were given a 4-week recovery period and to allow for AAV2 expression. These 2 groups of mice were then placed on either the HFD or LFD for 6 weeks, as above (Supplemental Figure 2B). In LFD-fed male mice, deletion of PRR from PVNTH neurons once again had no significant effect on body weight (Supplemental Figure 2C), caloric intake (Supplemental Figure 2D), FBG (Supplemental Figure 2E), or glucose tolerance (Supplemental Figure 2, F–H). Compared with their lean counterparts, the 6-week HFD regimen in male mice resulted in the expected increase of body weight (Supplemental Figure 2C), calorie intake (Supplemental Figure 2D), and FBG levels (Supplemental Figure 2E), along with impaired glucose tolerance (Supplemental Figure 2, F–H). Despite exhibiting similar increases in body weight and calorie intake as HFD-Control mice (Supplemental Figure 2, C and D), HFD-PVNTH-PRRKO mice once again had lower FBG levels (Supplemental Figure 2E) and improved glucose tolerance (Supplemental Figure 2H) compared with HFD-control mice. These data confirm that, in male DIO mice, the beneficial effect of PRR deletion in the PVNTH neurons is evident irrespective of the presence of the tdTomato reporter.

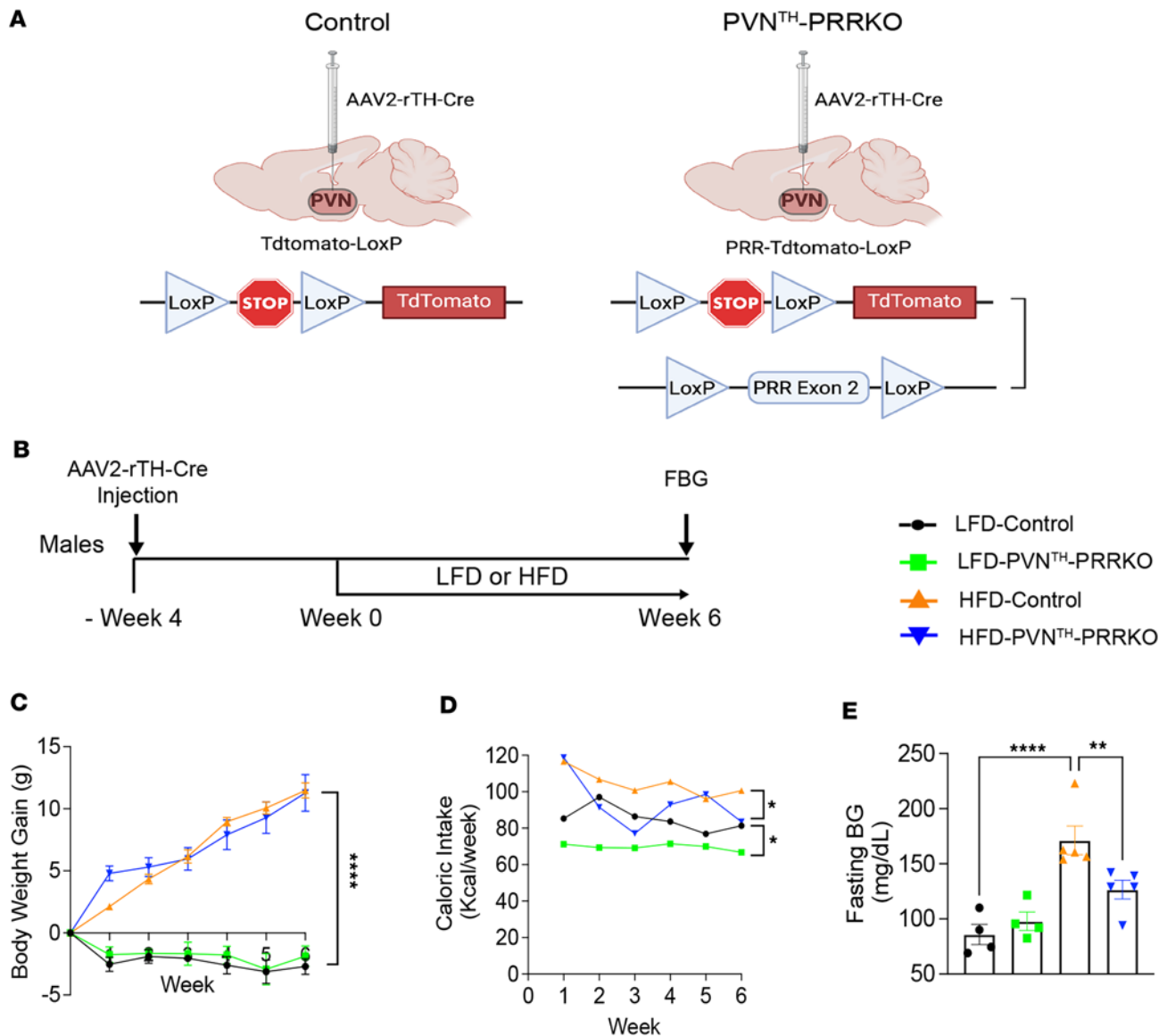


Figure 3. Deletion of (pro)renin receptor (PRR) in PVNTH neurons lowers fasting blood glucose (FBG) in HFD-induced obese male mice. (A) Schematic representation of Cre-LoxP-mediated deletion of PRR in PVNTH neurons in PRR-tdTomato-LoxP mice. Mice bearing both PRR-LoxP and tdTomato-LoxP alleles (PRR-tdTomato-LoxP) received bilateral microinjection directed to the PVN of an AAV-expressing Cre recombinase driven by a rat tyrosine hydroxylase promoter (AAV2-rTH-Cre), while tdTomato-LoxP mice received the AAV2-rTH-Cre virus to the PVN and were used as controls. (B) Schematic diagram of the experimental protocol. Four weeks after viral injection, mice were placed on either a low-fat diet (LFD, 10% calories from fat) or a high-fat diet (HFD, 60% calories from fat). (C–E) Weekly body weight gain, calorie intake, and fasting blood glucose at 6 weeks following exposure to either an HFD or an LFD. $n = 4$ –5 animals/group. Data are expressed as mean \pm SEM. * $P < 0.05$, ** $P < 0.01$, **** $P < 0.0001$. Two-way ANOVA with Fisher's LSD multiple comparisons tests were used.

To evaluate the possibility of a sex effect on this phenotype, we repeated the above studies in female mice (either with or without a tdTomato reporter). As a first step, PRR^{f/f} mice received a bilateral microinjection into the PVN of either a control virus (AAV2-TH-GFP) or AAV2-rTH-Cre to delete PRR in PVNTH neurons (Supplemental Figure 3A) and were placed on LFD or HFD after 4 weeks of recovery (Supplemental Figure 3B). In LFD-fed female mice, PRR deletion from PVNTH neurons had no significant effect on FBG (Supplemental Figure 3C) or glucose tolerance (Supplemental Figure 3, D–F), as expected. Exposure to the HFD for 6 weeks significantly elevated FBG (Supplemental Figure 3C) but did not impair glucose tolerance in these female mice (Supplemental Figure 3, D–F) relative to LFD-Control; unlike in males, PRR deletion from PVNTH neurons had no effect on either FBG (Supplemental Figure 3C) or glucose tolerance (Supplemental Figure 3, D–F) relative to controls. We also observed no

effect of selective deletion of PRR from PVNTH neurons on either body weight or food intake in either LFD or HFD-fed mice.

To confirm these findings in females, and to examine whether the effect of PVNTH-PRRKO is background or strain dependent, the studies were repeated in female PRR-tdTomato-LoxP mice and female tdTomato-LoxP mice controls (Supplemental Figure 4, A and B). As was observed in female PRR^{fl/fl} mice, deletion of PRR from PVNTH neurons affected neither FBG (Supplemental Figure 4C) nor glucose tolerance in female mice fed the LFD (Supplemental Figure 4, D–F). Similarly, consuming the HFD for 6 weeks raised the FBG (Supplemental Figure 4C) but did not significantly impair glucose tolerance (Supplemental Figure 4, D–F) relative to female LFD-Control, and once again, deletion of PRR in PVNTH neurons in female mice had no effect on FBG (Supplemental Figure 4C) or glucose tolerance (Supplemental Figure 4, D–F) fed a HFD, unlike what was observed in males. Together, these findings suggest PPR signaling in PVNTH neurons exerts a sexually dimorphic effect, with glucose homeostasis being improved in male but not female HFD-fed mice.

Effect of selective deletion of PRR from PVNTH neurons on cardiovascular function and locomotor behavior. To determine the effect of PRR deletion in PVNTH neurons on cardiovascular parameters, telemetry transmitters were implanted into male mice to continuously monitor blood pressure, heart rate, and locomotor activity in freely moving conditions described previously (31, 34). As described earlier, both tdTomato-LoxP and PRR-tdTomato-LoxP mice underwent bilateral injection of AAV2-rTH-Cre into the PVN (Supplemental Figure 5A). Following telemetry transmitter implantation and recovery, cardiovascular parameters were recorded continuously at baseline and during 6 weeks of HFD treatment, as illustrated in Supplemental Figure 5B. At baseline (week 0), when mice were fed a regular chow diet, neither mean arterial blood pressure (Supplemental Figure 5, C and D) nor heart rate (Supplemental Figure 5, E and F) or locomotor activity (Supplemental Figure 5, G and H) differed between Control and the PVNTH-PRRKO mice. Within 1 week after switching to the HFD, mean arterial blood pressure (Supplemental Figure 5, C and D) and heart rate (Supplemental Figure 5, E and F) were increased during both the light cycle and dark cycle in all mice, and this effect persisted throughout the dietary regimen. However, these cardiovascular responses to the HFD were not significantly affected by PRR deletion from PVNTH neurons (Supplemental Figure 5, B–G). Similarly, no differences in locomotor activity were observed in response to the HFD in either group (Supplemental Figure 5, G and H). Collectively, these findings show that, in male mice, the deleterious effects of HFD on glucose homeostasis, but not on body weight, blood pressure, or heart rate, were ameliorated by PRR deletion, specifically from PVNTH neurons.

Effects of PRR signaling on insulin secretion, insulin sensitivity, and insulin-independent glucose disposal. To explore the peripheral mechanisms underlying the beneficial effects on glucose homeostasis, we performed a frequently sampled i.v. glucose tolerance test (FSIGT) on male DIO mice with or without PRR deletion from PVNTH neurons. This method was chosen because, unlike other phenotyping methods, the FSIGT quantifies both glucose tolerance and glucose-induced insulin secretion (acute insulin response to glucose AIR_G) while also deriving validated estimates (35) of both insulin sensitivity index (S_I) and insulin-independent glucose uptake (S_G) from minimal model analysis of plasma insulin and glucose levels.

Studies were performed following bilateral injection to the PVN of an AAV2-rTH-Cre virus in male mice bearing either the PRR-floxed allele and the loxP-flanked STOP cassette for tdTomato or only the loxP-flanked STOP cassette for tdTomato (Figure 4A), as described above. Mice were then subjected to an FSIGT after consuming the HFD for 6 weeks and undergoing arterial and venous catheterization (Figure 4B). As predicted, glucose tolerance was improved in male HFD-PVNTH-PRRKO mice compared with DIO-Controls (Figure 4, C–E). Surprisingly, plasma insulin levels tended to be lower in the HFD-PVNTH-PRRKO mice than in HFD-Controls, although this effect did not achieve statistical significance (except at the 20-minute mark after glucose injection; Figure 4, F–I). Nevertheless, combined with the finding of no difference in the acute insulin response to glucose (AIR_G) between the 2 groups, we infer that improved glucose tolerance in PRR-deleted mice is not due to increased insulin secretion. By comparison, fasting plasma glucagon levels were significantly reduced by PRR deletion PVNTH neurons from (Figure 4J), which could have played a role by reducing hepatic glucose production (36, 37).

Minimal model analysis of plasma glucose and insulin levels obtained during the FSIGT (35, 38, 39) did not identify statistically significant differences between the 2 groups in any parameter. Nevertheless, the tendency for the S_I to be higher in HFD-fed mice in which PRR was deleted from PVNTH neurons than in controls (Figure 4K) suggests that increased insulin sensitivity could have contributed to the observed

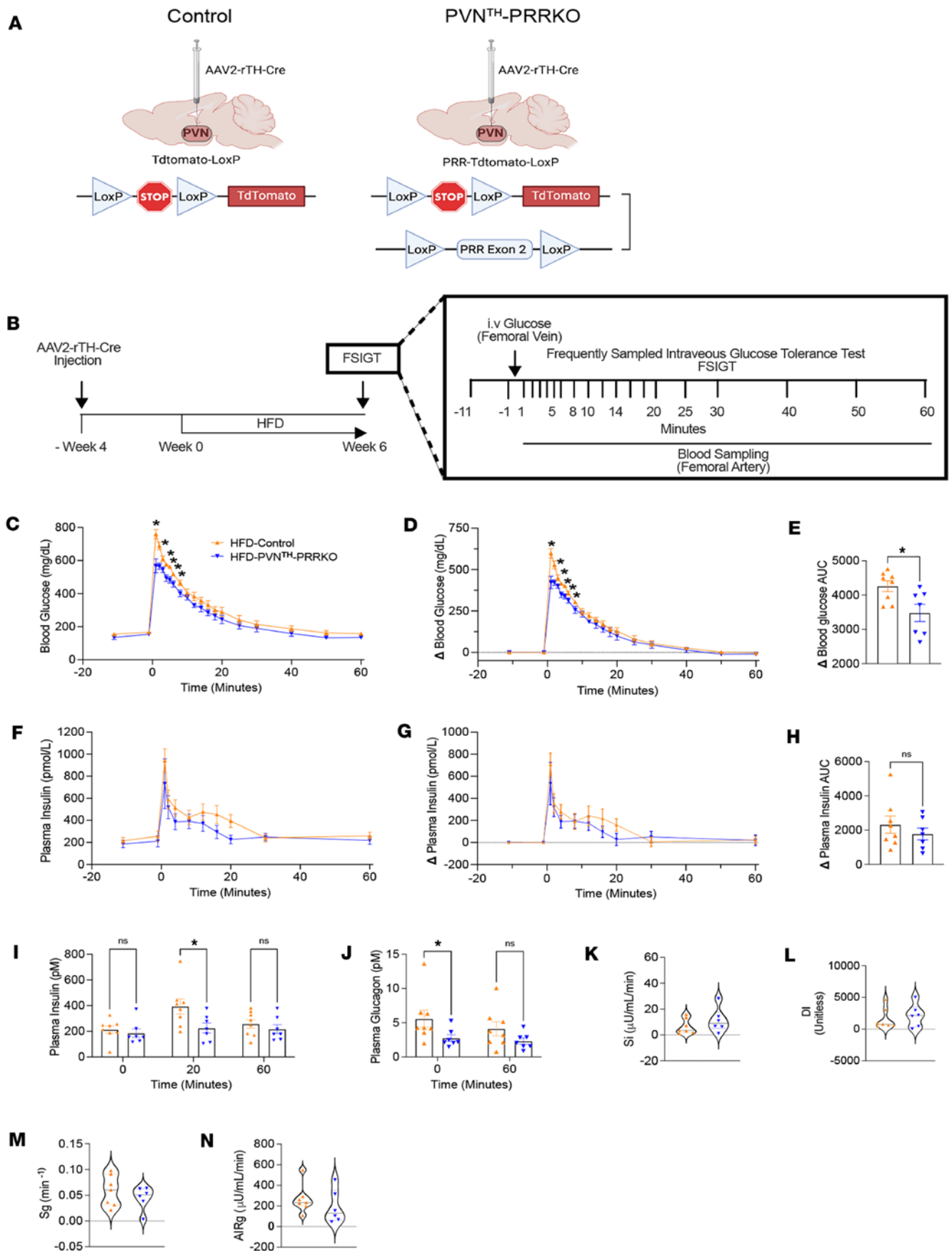


Figure 4. Effects of (pro)renin receptor (PRR) deletion in PVNTH neurons on determinants of glucose tolerance. (A) Schematic representation of Cre-LoxP-mediated deletion of PRR in PVNTH neurons in PRR-tdTomato-LoxP mice. AAV-expressing Cre recombinase driven by a rat tyrosine hydroxylase promoter (AAV2-rTH-Cre) was used to delete PRR and induce tdTomato reporter expression in mice bearing both PRR-LoxP and tdTomato-LoxP alleles, shown as PVNTH-PRRKO. The tdTomato-LoxP mice that received the AAV2-rTH-Cre were used as controls. (B) Schematic diagram of the experimental protocol. Mice received a high-fat diet (HFD, 60% calories from fat) for 6 weeks. (C–E) Blood glucose levels, changes in blood glucose levels, and glucose AUC from baseline during the FSIGT. (F–H) Plasma insulin levels, changes in plasma insulin levels from baseline, and respective insulin AUC during FSIGT. (I and J) Plasma insulin levels ($t = 0, 20, 60$ min) and glucagon levels ($t = 0, 60$ min) during the FSIGT. (K–N) Insulin sensitivity (S_i), disposition index (D_i), glucose effectiveness (S_G), and acute insulin response to glucose ($AI R_G$) were analyzed from plasma insulin and glucose profiles during FSIGT using MINMOD Millennium software. $n = 6$ –7 mice/group. Data are expressed as mean \pm SEM. * $P < 0.05$, 2-way ANOVA followed by Fisher's LSD tests for **D, F, G, I, and J**; unpaired t test for **E** and **H**; unpaired Mann-Whitney test for **K–N**.

improvement of glucose tolerance, and additional studies are warranted to test this hypothesis. In addition, neither the disposition index (D_i) nor glucose effectiveness (S_G ; a measure of insulin-independent glucose disposal) (Figure 4, L–N) differed significantly between groups. These findings suggest that, in DIO mice, PRR signaling in PVNTH neurons impairs glucose tolerance via a mechanism that, while not involving decreased insulin secretion, may involve reduced insulin sensitivity. Additional studies are warranted to test this hypothesis.

PVNTH neurons are inhibited by PRR activation. To better understand cellular mechanisms through which PRR signaling influences PVNTH neurons, we performed slice electrophysiology on TH⁺ neurons identified in the PVN of both male and female TH-Cre-driven tdTomato reporter mice. Specifically, cell-attached patch-clamp electrophysiology was used to measure the effect of the application of the PRR agonist prorenin on PVNTH neuron activity. To exclude any potential effect of prorenin on neurons lying upstream, these studies were performed in the presence of synaptic transmission blockers (Figure 5A). We found that, following bath application of prorenin, the spontaneous firing rate (SFR) of PVNTH neurons was reduced by $\sim 30\%$ compared with artificial cerebrospinal fluid (aCSF) control (Figure 5, B–D). To validate the specificity of this effect, we repeated this study in both the presence and absence of PRO20, a specific PRR antagonist (19). Our finding that PRO20 fully blocked the effect of prorenin on PVNTH neuron firing rate (Figure 5, E–G) indicates that PRR activation is required for the inhibitory effect of prorenin on PVNTH neurons. Experiments conducted on brain slices from mice lacking PRR, specifically in the PVNTH neurons, yielded similarly negative findings (Figure 5, H–K), confirming that the PRR must be expressed by PVNTH neurons for these neurons to be inhibited by prorenin. Future studies are needed to identify the signal transduction mechanisms underlying this inhibitory effect.

Chemogenetic inhibition of PVNTH neurons elevates blood glucose in mice. Since selective deletion of the PRR from PVNTH neurons blocks the deleterious effect of DIO on glucose homeostasis, and since PVNTH neurons are inhibited by PRR activation, we next tested the hypothesis that, in mice fed standard chow, chemogenetic inhibition of PVNTH neurons would mimic the deleterious effect of DIO to impair glucose homeostasis. To this end, we combined designer receptors exclusively activated by designer drugs (DREADD) technology with continuous telemetric glucose monitoring in both male and female mice engineered to express inhibitory human M4 muscarinic receptors (hM4Di) on TH-expressing neurons. For the non-DREADD control group, non-Cre (GFP) virus-infected mice were used (Figure 6A).

Upon i.p. administration of saline vehicle, a rapid but transient elevation of blood glucose levels was observed, presumably the result of a nonspecific stress response. In contrast, i.p. administration of the DREADD receptor agonist CNO (1 mg/kg) elicited a notable elevation of blood glucose levels that persisted throughout the 3-hour monitoring period (compared with controls) in both male and female mice (Figure 6, B–F). Consistent with our earlier findings, we observed that, when segregating data by sex, male mice (Figure 6, C and D) exhibited a much greater glycemic elevation than females in response to PVNTH neuron inhibition (Figure 6, E and F). A similar set of responses was observed in the DIO model. To exclude the possibility that this increase in glycemia was due to nonspecific CNO effects (unrelated to PVNTH neuron inhibition), we replicated the experiment in non-DREADD control mice. While the initial, transient rise of blood glucose was once again observed following the i.p. injection of either vehicle or CNO (Figure 6G), no sustained elevation of glycemia was observed in response to CNO administration (Figure 6, H and I). Collectively, these data establish that chemogenetic inhibition of PVNTH neurons raises the blood glucose level.

PVNTH neurons project to autonomic and neuroendocrine regulatory brain regions. To identify projections of PVNTH neurons to brainstem autonomic regulatory nuclei, we microinjected AAV2-rTH-Cre into the PVN of Cre-dependent GFP reporter mice (Figure 7A), which labels both cell bodies and projecting fibers with GFP

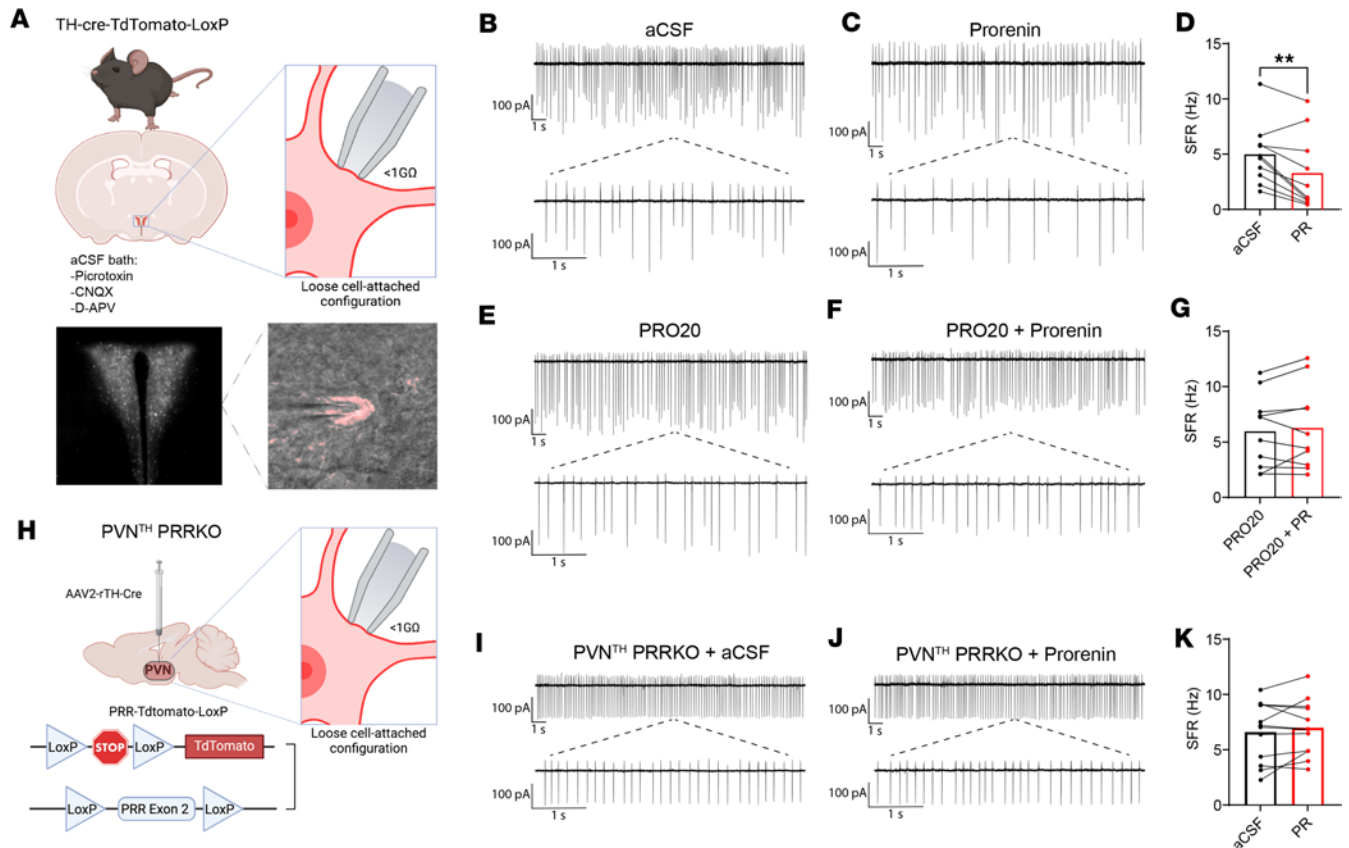


Figure 5. Prorenin decreases the spontaneous firing rate of PVNTH neurons. (A) Experimental illustration of a recorded PVNTH neuron under loose cell-attached configuration in the presence of blockers of synaptic transmission. Picrotoxin, 50 μ M; antagonist of AMPA/kainate receptors, CNQX, 5 μ M; NMDA receptor antagonist, D-APV, 50 μ M. (B and C) Representative raw traces of loose cell-attached recordings of spontaneous firing activity in a PVNTH neuron in aCSF or 2.5 nM prorenin (PR). (D) Summary data of spontaneous firing rate (SFR) showing that application of PR decreased SFR of PVNTH neurons ($n = 7$ mice/10 neurons). (E and F) Representative raw traces of loose cell-attached recordings of spontaneous firing activity in a PVNTH neuron in the presence of 250 nM PRO20, a specific (pro)renin receptor (PRR) antagonist, and PRO20 + PR. (G) Summary data of SFR of PVNTH neurons in the presence of PRO20 ($n = 7$ mice/10 neurons). (H) Schematic representation of Cre-LoxP-mediated deletion of PRR in PVNTH neurons in PRR-TdTomato-LoxP mice. (I and J) Representative raw traces of loose cell-attached recordings of spontaneous firing activity in a PVNTH neuron from a PVNTH PRRKO mouse. (K) Summary data of SFR showing that PR did not affect the SFR of PVNTH neurons in PVNTH PRRKO mice ($n = 6$ mice/12 neurons). Data are obtained from both male and female mice and are expressed as mean \pm SEM. $**P < 0.01$, 2-tailed paired Student's t test was used.

(Figure 7B). Whereas projections to the cerebral cortex (Figure 7C) or forebrain regions such as the subfornical organ (SFO) were not observed (Figure 7D), dense projections to the median eminence (ME; Figure 7E) and nucleus of the solitary tract (NTS; Figure 7F) were evident. To a lesser extent, projections to the dorsal motor nucleus of the vagus (DMV; Figure 7F) and rostral ventrolateral medulla (RVLM; Figure 7G) were also observed. Based on these findings, we generated a schematic that illustrates descending PVNTH neuronal projections (Figure 7H), with thicker lines representing denser projections. Based on this anatomical evidence that TH^{PVN} neurons project to brain regions regulating endocrine and autonomic function (40–42), we hypothesize that, during DIO, impaired glucose tolerance and elevated FBG levels result at least in part from inhibition of PVNTH neurons mediated by PRR activation (Figure 7I). As noted earlier, these effects occur independently of changes in body weight.

Discussion

Our work demonstrates first that the PRR is expressed in the vast majority of PVNTH neurons, and that PRR signaling exerts an inhibitory effect on these neurons. Using a chemogenetic approach, we further show that glucose homeostasis is impaired by inhibition of PVNTH neurons in a manner resembling the effect of DIO, whereas deletion of the PRR, specifically from PVNTH neurons, blunts the deleterious effect of DIO on glucose homeostasis. Furthermore, these effects are mediated via a mechanism that does not involve differences in body weight, is not associated with changes in heart rate or blood pressure, and appears to be specific for

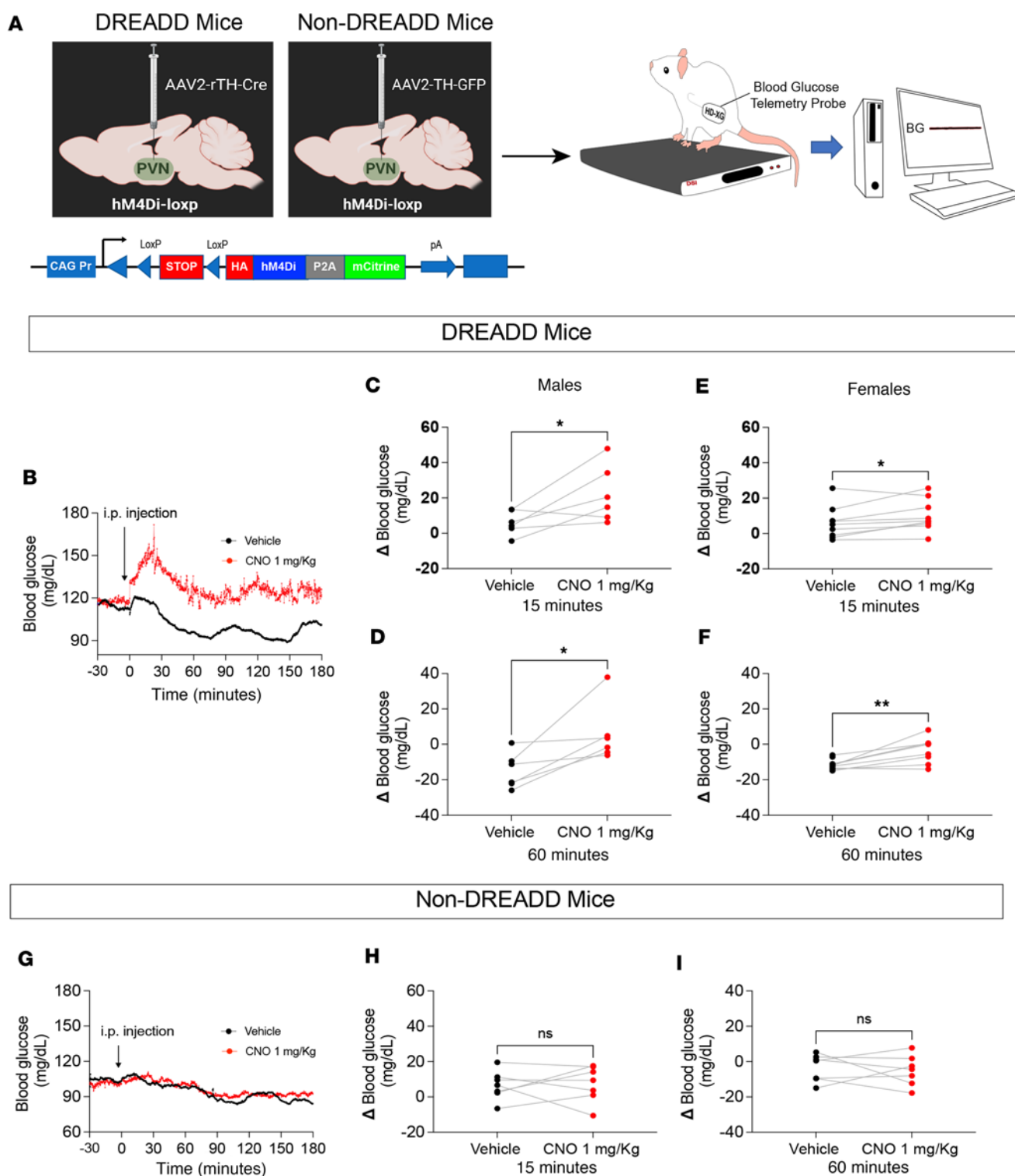


Figure 6. Chemogenetic inhibition of PVNTH neurons increases blood glucose in both male and female mice. (A) Schematic diagram of 1-time injections of either AAV2-TH-GFP (control virus, non-DREADD) or AAV2-rTH-Cre (DREADD) into the PVN of hM4Di-LoxP mice. One month after the AAV2 injection, mice were implanted with HD-XG telemetric glucose transmitters followed by continuous glucose monitoring (CGM). (B) Representative traces of CGM following injection of either vehicle or clozapine N-oxide (CNO, 1 mg/Kg) for 3 hours in DREADD mice. (C and D) Summary data of blood glucose levels following injection of either vehicle or CNO at 15 and 60 minutes in male mice ($n = 6$). (E and F) Summary data of blood glucose levels following injection of either vehicle or CNO at 15 and 60 minutes in female mice ($n = 9$). (G) Representative traces of CGM following injection of either vehicle or clozapine N-oxide (CNO, 1 mg/Kg) for 3 hours in non-DREADD mice. (H and I) Summary data of blood glucose levels following injection of either vehicle or CNO at 15 and 60 minutes in both male ($n = 3$) and female ($n = 4$) non-DREADD mice. Data are expressed as mean \pm SEM. * $P < 0.05$, ** $P < 0.01$, 2-tailed paired Student's t test was used.

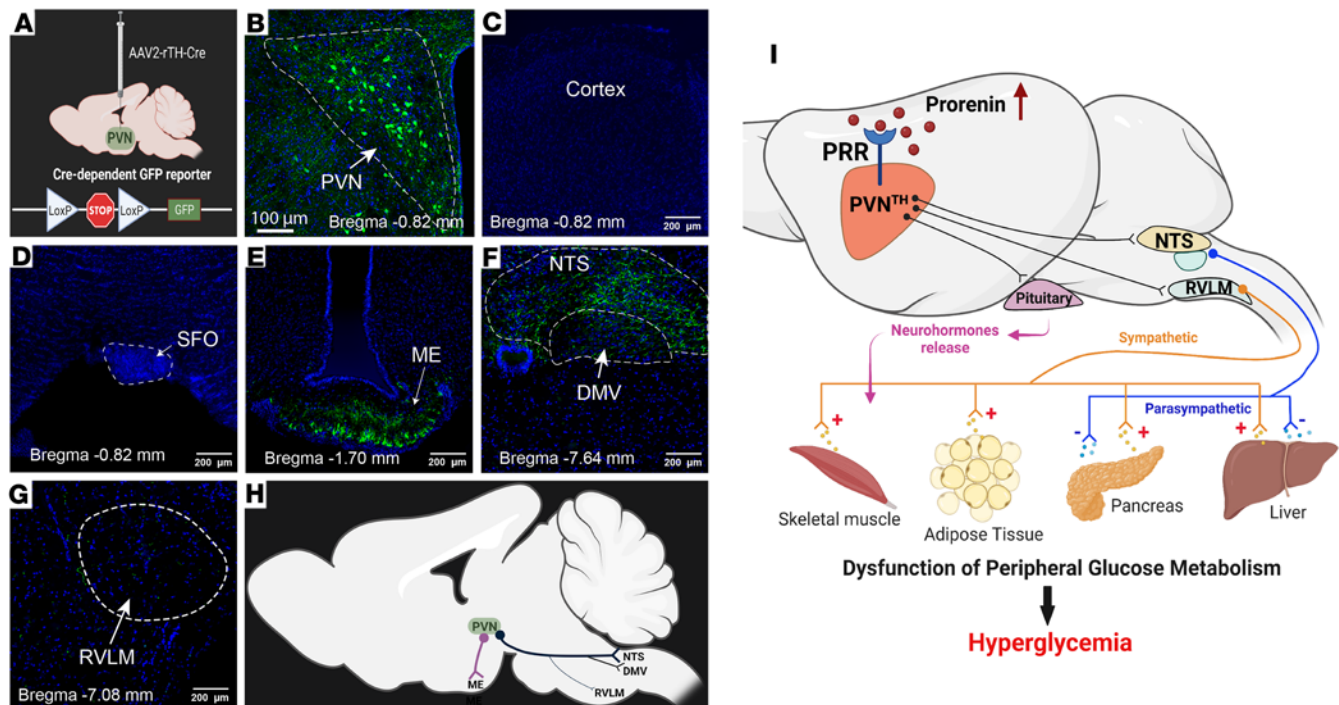


Figure 7. Anatomical mapping of tyrosine hydroxylase neurons (PVNTH) in the hypothalamic paraventricular nucleus and the working hypothesis. (A) Schematic representation of Cre-mediated deletion Flox-STOP in Cre-dependent GFP^{fl/fl} mice. AAV-expressing Cre recombinase driven by a rat tyrosine hydroxylase promoter (AAV2-rTH-Cre) was bilaterally injected into the PVNs of Cre-dependent GFP^{fl/fl} mice. (B–G) Representative images of PVN (B), brain cortex (C), subfornical organ (SFO; D), median eminence (ME; E), the nucleus of the solitary tract (NTS; F), the dorsal motor nucleus of the vagus (DMV; F), and the rostral ventrolateral medulla (RVLM; G). (H) A schematic summary of the PVNTH neuronal projection map. The thicker lines represent denser projections, and the thinner lines represent lesser projections. *n* = 4 mice. (I) Working hypothesis. During diet-induced obesity, (pro)renin receptor (PRR) signaling activation in the tyrosine hydroxylase neurons in the hypothalamic paraventricular nucleus leads to inhibition of these PVNTH neurons and, consequently, the dysregulation of peripheral glucose homeostasis by neural autonomic and/or neuroendocrine mechanisms.

male mice. Together, these findings suggest that, in male mice, PVNTH neuron activity is required for normal glucose homeostasis under physiological conditions and that inhibition of these neurons by increased PRR signaling contributes to obesity-associated impairment of glucose homeostasis.

The hypothalamic PVN comprises multiple neuronal subpopulations, including many neuroendocrine and preautonomic neurons that play critical roles in various physiological processes (43–45), including glucose homeostasis (46). Compared with PVN neurons involved in the control of the hypothalamic-pituitary-adrenal and hypothalamic-pituitary-thyroid axes (expressing CRH and TRH, respectively), as well as neurons expressing oxytocin or vasopressin, however, TH-containing neurons in this brain area have received limited attention. Most of these neurons appear to be both GABAergic and dopaminergic (10), and they have been suggested to participate in the control of sympathetic activity to brown adipose tissue (BAT) (11). Their role in glucose homeostasis, however, remains unexplored.

Based on our finding that the blood glucose level is rapidly elevated following their chemogenetic inhibition, PVNTH neurons join the growing list of hypothalamic neurons implicated as contributors to the biologically defended level of glycemia (3, 46). We also present electrophysiological evidence that PRR activation exerts a direct, inhibitory effect on PVNTH neurons that does not require synaptic transmission. Combined with our finding that the deleterious effects of DIO on both the circulating glucose level and glucose tolerance are ameliorated by PRR deletion from PVNTH neurons, we infer a role for PRR signaling in these neurons in the pathogenesis of obesity-associated glucose metabolic impairment. Interestingly, this effect occurs independently of changes in food intake, body weight, blood pressure, or heart rate, suggesting a high degree of functional specificity. Questions that remain to be addressed include whether experimental activation of PVNTH neurons can blunt the effect of obesity to impair glucose tolerance and the ways in which PRR signaling and the activity of these neurons are affected by DIO.

The PRR (18) is an essential component of the brain RAS that regulates blood pressure, heart rate, and other cardiovascular functions (16, 17). In addition to the local generation of Ang II, which binds to

and activates neuronal angiotensin receptors, binding of the PRR by either of its 2 endogenous ligands (prorenin or renin) activates an intracellular tyrosine kinase signal transduction cascade (16, 47). Interestingly, while activation of neuronal PRR signaling has been shown to promote hypertension development by increasing vasopressin release (30, 32, 48, 49), we report that only a small percentage of PVNTH neurons express vasopressin. Indeed, our work suggests little, if any, role of PRR signaling in PVNTH neurons in cardiovascular regulation.

Recently, a role for brain RAS activity in the control of energy balance has been suggested (14, 15). Specifically, intracerebroventricular (ICV) administration of Ang II reduces food consumption, body weight, and adipose tissue mass while simultaneously increasing thermogenesis in BAT, lipolysis in white adipose tissue (WAT), and overall energy expenditure in rats (50, 51). Deletion of Ang II type 1a receptor (AT_{1a}R), specifically in leptin receptor-expressing neurons, also inhibits the increase of resting metabolic rate that occurs as a response to an HFD (52). Interestingly, we showed that PRR deletion in the PVNTH neurons does not affect food intake or body weight; instead, it attenuates the glucose metabolic impairment induced by consuming an HFD. Whether this effect involves the local generation of Ang II awaits further study; the data together are suggestive of brain region- or cell type-specific effects of brain RAS across various aspects of fuel homeostasis.

Interestingly, we observed that PRR deletion in the PVNTH neurons does not improve the glucose metabolic phenotype in female mice. Moreover, although chemogenetic inhibition of PVNTH neurons raised the blood glucose level in both sexes, the effect was much smaller in females (~4 mg/dL) than in their male counterparts (~17 mg/dL). Together, these findings suggest a more prominent role of PVNTH neurons in the control of glucose homeostasis in males. Interestingly, however, ex vivo electrophysiological analysis did not reveal a sex difference in the inhibitory effect of PRR activation on PVNTH neuron activity. Thus, we infer that the sex difference is not localized to a failure of PVNTH neurons to respond to PRR activation in females; more likely, the sex difference in phenotype involves circuits lying downstream of these neurons. Given that CNS control of glucose homeostasis involves a complex network of glucoregulatory circuits, it is perhaps unsurprising that this system can be modulated by variables including sex. In this context, we note that male mice tend to be more prone to obesity-associated metabolic impairment than females; future studies that focus on the identification of these downstream neurocircuits will eventually permit investigation into whether they are regulated by PRR signaling in PVNTH neurons in a sex-dependent manner.

While the peripheral mechanism whereby PRR deletion from PVNTH neurons lowers blood glucose and improves glucose tolerance in male mice remains uncertain, our work excludes increased insulin secretion as a key factor. More likely is that the effect involves increased insulin sensitivity, possibly via changes in autonomic outflow and HPA axis activity secretion, in addition to our finding of reduced glucagon levels, expected to lower hepatic glucose production (36, 37). Future studies to investigate whether increased PVNTH neuron activity inhibits glucagon secretion from pancreatic α cells (4, 38, 53) will be of interest.

One limitation of the current studies is that, while all animals received bilateral PVN injections, a small subset of mice was “hit” unilaterally, there were differences in the spread of viral injection throughout the rostral-caudal extent of the PVN, and there was a small amount of spillover, targeting TH neurons near the PVN. Thus, we cannot exclude a potential contribution of our observations made by these TH neurons. However, our findings were consistent across multiple studies, supporting the conclusions drawn on the effect of PRR, although future studies are warranted to identify the distinct subset of PVNTH-PRR neurons that mediate the observed phenotype. In summary, our data identify PVNTH neurons as participants in CNS regulation of glucose homeostasis and implicates PRR-mediated inhibition of these neurons in the pathogenesis of obesity-associated glucose metabolic impairment.

Methods

Sex as a biological variable. Both male and female mice were used in the study.

Animals. Mice in a C57BL/6J genetic background were used in this study, except for TH^{Cre+} and hM4Di^{fl/fl} mice, which are in a C57BL/6NJ background. The C57BL/6J mice (stock no. 000664), GFP^{fl/fl} mice (stock no. 030220) (54), TH^{Cre/+} mice (stock no. 008601) (55), tdTomato^{fl/fl} (stock no. 007914) (56), and human muscarinic receptor 4 coupled to Gi protein hM4Di^{fl/fl} (stock no. 026219) (57) were purchased from The Jackson Laboratory. The PRR-LoxP (male, PRR^{fl/y}; female, PRR^{fl/fl}) mice were maintained in the Feng Earley laboratory (University of Nevada, Reno) (20). The PRR-LoxP mice were crossed with the tdTomato^{fl/fl} for a few generations to generate double-LoxP mice for PRR and tdTomato (PRR-tdTomato-LoxP). Hemizygous

TH^{Cre+} mice were crossed with tdTomato^{fl/fl} mice to generate reporter mice that express tdTomato in TH⁺ cells (TH^{Cre+}tdTomato^{fl/+}).

All mice were maintained in the Animal Care Facility at the University of Nevada, Reno, under a 12-hour light-dark cycle and room temperature of 21°C–23°C with ad libitum access to a standard chow diet (Envigo, catalog 2019) before other diet regimens.

RNA*Scope* in situ hybridization. In situ hybridization of TH and PRR mRNAs was performed using an RNA*Scope* Multiplex Fluorescent Assay kit (ACD Inc.) together with a specific probe complementary to a section of the mouse TH (NCBI Gene ID: 21823, ACD, 317621), PRR (NCBI Gene ID: 70495, ACD, 429931), and vasopressin (NCBI Gene ID: 11998, ACD, 401391) mRNA sequences. As a negative control, we used a probe for the bacterial gene 4-hydroxy-tetrahydrodipicolinate reductase (DapB) (NCBI Gene ID: EF191515, ACD, 310043). For RNA*Scope* assays, WT C57Bl/6J mice ($n = 3$ –6/group) were transcardially perfused first with 0.9% saline and then with 4% paraformaldehyde (PFA; Sigma-Aldrich). Thereafter, brains were immediately extracted and kept in 4% PFA for 24 hours at 4°C and then cryoprotected in 30% sucrose solution for an additional 24 hours at 4°C. Brains were frozen at –20°C in Tissue Freezing Medium (EMS, 72592) for 12 hours before sectioning. PVN-containing coronal sections (30 μ m thickness) were cut using a cryotome (Leica CM1950) at –24°C. Sections were floated in PBS 1 \times containing 0.1% sodium azide as conservative at 4°C until used. Sections were then mounted onto Colorfrost Plus slides (Thermo Fisher Scientific, 12-550-18) and dried at –20°C for 30 minutes. The standard RNA*Scope* protocol for fixed frozen tissues (ACD User Manual 323100-USM) was followed with minor modifications. A HybEZ II Hybridization System (ACD Inc.) was used to control incubation temperature. Briefly, slides were baked at 60°C for 25 minutes, before being fixed in PFA for 15 minutes at 4°C, followed by dehydration with a graded series of ethanol (50%, 70%, and 100%) for 5 minutes each at room temperature. A hydrophobic barrier was drawn surrounding the mounted tissue, and sections were incubated in 3% hydrogen peroxide for 10 minutes at room temperature and rinsed in distilled H₂O. Target retrieval was performed by steaming slides (Hamilton Beach 37530A steamer) for 5 minutes. Slides were reimmersed in 100% ethanol for 3 minutes and air dried at room temperature. Sections were then incubated with Protease III for 30 minutes at 40°C. Excess liquid was removed from the slide, and sections were incubated with either a mixture of TH and PRR probes or negative control probe (DapB); slides were incubated at 40°C for 2 hours. For signal amplification, slides were incubated with AMP1 (30 minutes), AMP2 (30 minutes), and AMP3 (15 minutes) (ACD, 320851) at 40°C, with thorough washes in 1 \times wash buffer between steps. After amplification, a horseradish peroxidase–conjugated (HRP-conjugated) probe of interest was applied and incubated for 15 minutes at 40°C. This was followed by a 30-minute incubation at 40°C with fluorescein (1:250 dilution) for PRR and Cyanine 5 (1:250 dilution) for TH, followed by a 15-minute incubation with an HRP blocker at 40°C. Cell nuclei were counterstained with DAPI, after which sections were mounted and covered with glass slip using Prolong Gold Antifade Mountant (Thermo Fisher Scientific, P36930) and imaged using a confocal microscope (Leica Stellaris 8).

All images were acquired at a resolution of 1,024 \times 1,024 with a pixel speed of 600 Hz. Pinhole, laser power, and gain were optimized and kept consistent for all slides, including negative control slides. For cell counting analysis, at least 4 images from each mouse with similar coronal levels covering rostral (bregma, –0.58 mm) to caudal (bregma, –1.22 mm) PVN were used for RNA*Scope* as described above. Cells were considered to express the mRNA of interest if at least 3 visible transcripts, defined as an individual punctate dot, were observed surrounding a nucleus (58). Individual cells were identified using DAPI. Cell count and colocalization analysis were manually performed using Adobe Photoshop.

Bilateral nanoinjection of AAVs into the PVN. Mice were anesthetized using 4%–5% isoflurane in 100% O₂ and flushed at 1 L/min for 2 minutes, and anesthesia was subsequently maintained using 1.5% isoflurane. The top of each mouse's head was shaved and sterilized with alcohol wipes, after which the mouse was placed in a digital stereotaxic apparatus (Stoelting) and held in place by ear bars secured just above the ear canal. Heads of mice were then sterilized with alcohol wipes, and an incision (~2 cm) in the skin along the top of each head was made to expose the skull. The skull was cleaned with 3% hydrogen peroxide using cotton swabs, after which holes were drilled into the skull, and bilateral nanoinjections of viral constructs were performed at the stereotaxic coordinates, 0.6 mm posterior, \pm 0.3 mm lateral, and 5.4 mm ventral to bregma. A 1 μ L Neuros Hamilton syringe (32 gauge) attached to a UMP3 syringe pump (WPI) was fixed to the stereotaxic frame and used for AAV nanoinjections at a rate of 5 nL/s for 15 minutes for a total injection volume of 75 nL. After each injection to the PVN, the syringe needle was left in place for an additional

5 minutes before removing it to prevent backflow of the virus through the needle track. The wound was sutured, and postoperation analgesics (SR Buprenex, 0.6 mg/kg, s.c.) were administered. Mice were allowed 4 weeks to recover from surgery and to allow for the expression of AAV2.

For the PVNTH-PRRKO study, mice bearing both PRR-LoxP and tdTomato-LoxP alleles (PRR-tdTomato-LoxP mice) received a bilateral microinjection directed to the PVN of an AAV-expressing Cre-recombinase driven by a rat TH reporter (AAV2-rTH-Cre; 1.88×10^8 vg in 75 nL, Vector Biolabs), while tdTomato-LoxP control mice lacking the floxed PRR allele underwent the same AAV2-rTH-Cre virus injection protocol and were used as controls (Figure 2A and Figure 3A). A complementary, second PVNTH-PRRKO study was performed in mice lacking the tdTomato reporter. Here, PRR^{fl/fl} mice received a bilateral microinjection to the PVN of either a control virus (AAV2-TH-GFP) or AAV2-rTH-Cre to delete PRR in PVNTH neurons (Supplemental Figure 2A). For the chemogenetic study, hM4Di^{fl/fl} mice received bilateral stereotaxic injections to the PVN of either AAV2-TH-GFP (6.8×10^8 vg in 136 nL, Vector Biolabs) as a control or AAV2-rTH-Cre (6.8×10^8 vg in 272 nL, Vector Biolabs) to induce the expression of hM4Di in TH⁺ cells in the PVN. For mapping of PVNTH neuronal projections, the GFP^{fl/fl} mice received a unilateral microinjection of AAV2-rTH-Cre (1.88×10^8 vg in 75 nL, Vector Biolabs) directed to the PVN. Injection sites were confirmed at the end of each study by localizing fluorescence reporters. A mouse is defined as correctly targeted when the fluorescence reporter was observed in at least two-thirds of the PVN ranging from bregma -0.58 mm to -1.22 mm. Mice with either bilateral or unilateral targeting of PVN were included in the data analysis. In only a single mouse, viral microinjection failed to target PVN; this animal was excluded from further analysis.

Fluorescent immunolabeling of PRR. The PRR-tdTomato-LoxP mice and the tdTomato-LoxP mice used as control received a bilateral injection of AAV2-rTH-Cre virus as described above. Four weeks after the AAV2 injection, mice were transcardially perfused first with 0.9% saline and then with 4% PFA (Sigma-Aldrich). Thereafter, brains were extracted and kept in 4% PFA for 24 hours at 4°C and were then cryoprotected in 30% sucrose solution for an additional 24 hours at 4°C. Brains were frozen at -20°C in Tissue Freezing Medium (EMS, 72592) for 12 hours before sectioning. PVN-containing coronal sections (30 μm thickness) were cut using a cryotome (Leica CM1950) at -24°C . Sections were floated in PBS 1 \times containing 0.1% sodium azide as conservative at 4°C until used. Sections were blocked by incubation in 500 μL of PBST containing 10% normal goat serum for 1 hour at room temperature before incubation in primary anti-PRR antibody (NBP1-33605, Novus Biologicals) for 48 hours, diluted 1:100. Slices were then washed 3 times in PBS for 5 minutes each, followed by a 2-hour incubation with Alexa Fluor 488-conjugated goat anti-rabbit secondary antibody (A-11008, Invitrogen, Thermo Fisher Scientific), diluted 1:1,000 in PBST containing 2% normal goat serum. Slices were washed twice in PBS and incubated with DAPI (1:1,000) for 5 minutes. After 2 washes in PBS, slices were mounted on microscope slides and coverslipped using a fluorescent mounting medium (Vector Biosciences). Slides were light protected and allowed to dry overnight; they were imaged using a confocal microscope (Leica Stellaris 8). For data analysis, images from each mouse with similar coronal levels covering rostral (bregma, -0.58 mm) to caudal (bregma, -1.22 mm) PVN were used and analyzed by ImageJ (NIH; version: 2.1.0/1.53c) to identify the red tdTomato⁺ cells and the fluorescence intensity of the PRR immunolabeling in each tdTomato⁺ cell. The mean PRR fluorescence intensity of each tdTomato⁺ cell from 1 PVN was presented as 1 datum.

Experimental model of DIO. Mice were single-housed and fed a HFD (catalog D12492) or a matched LFD (catalog D12450J) from Research Diets Inc. containing either 60% or 10% Kcal from fat, respectively, for 6 weeks. Body weight and food intake were monitored weekly.

FBG measurement. FBG measurements were obtained from all mice at the end of the 6-week treatment with either HFD or a control diet. Mice were transferred to clean cages and fasted for 16 hours (5:00 p.m. to 9:00 a.m.). Mice were then restrained in a dark tube, and blood was collected directly onto a blood glucose strip from a tail vein following a small tail snip performed using a razor. Glucose was then measured using a Bayer 7393A Contour blood glucose meter (Bayer). Two measurements were performed for each mouse using blood from a tail snip, and the average of the 2 values was used as the final measurement.

Glucose-tolerance test. A glucose-tolerance test (GTT) was performed at the end of the 6-week treatment with either HFD or a control diet. Mice were fasted for 16 hours (5:00 p.m. to 9:00 a.m.). Baseline blood glucose (0 minutes) was measured, and mice were then injected i.p. with glucose (1 g/kg body weight) and administered as a 10% glucose in a 0.9% saline formulation. Blood glucose was measured 15, 30, 60, 90, and 120 minutes following the injection of glucose using a Bayer blood glucose meter, as described for FBG experiments.

FSIGT. At the University of Nevada, Reno, mice received a bilateral injection of AAV2-rTH-Cre into the PVN as described above. After 4 weeks of recovery, allowing for virus expression. Mice received 60% HFD for 6 weeks and were transported to the University of Washington at week 4 of HFD. The FSIGT was performed in collaboration with the NIDDK-funded Diabetes Research Center Metabolic and Cellular Phenotyping Core at the University of Washington, as previously described (38, 39). Briefly, mice underwent carotid artery and jugular vein catheterization and recovered for 7 days prior to FSIGT in the conscious state. For FSIGT, mice were fasted for 5 hours, and blood was sampled through the arterial catheter at $t = -11$ minutes and -1 minute, after which a bolus of 50% dextrose (1 g/kg) was delivered at $t = 0$ minutes through the jugular vein. Thereafter, blood was sampled through the arterial catheter at $t = 1, 2, 3, 4, 5, 6, 8, 10, 12, 14, 16, 18, 20, 25, 30, 40, 50,$ and 60 minutes. Blood was measured using an Accu-Chek Aviva Plus glucometer (Roche). Plasma was collected for subsequent assay of insulin (Mouse Ultrasensitive Insulin ELISA, Alpco, 80-INSMSU-E01) and glucagon (Glucagon ELISA, Mercodia, 10-1281-01) levels. Experimental groups and treatment information were blinded to the Metabolic and Cellular Phenotyping Core staff. PVN targeting accuracy was not assessed in this cohort of animals, and no data were excluded from the analysis.

Minimal model analysis of FSIGT data. Plasma insulin and BG profiles during FSIGT were analyzed using MINMOD Millennium software to quantify insulin-independent glucose disposal, referred to as glucose effectiveness (S_G) and S_I , as previously described (38, 39, 59). The acute insulin response to glucose (AIR_G) was calculated as the mean increment above basal insulin values measured between $t = 0$ and 4 minutes. The disposition index was calculated as the product of S_I and AIR_G .

Electrophysiological studies. For PVN brain slice preparation, mice were anesthetized with ketamine (100 mg/kg; AmerisourceBergen) and xylazine (10 mg/kg; AmerisourceBergen) and sacrificed. Brains were quickly extracted from the skull and transferred into cold (4°C) aCSF containing (in mM): 124 NaCl, 1 MgSO₄, 5 KCl, 1.25 KH₂PO₄, 10 glucose, 26 NaHCO₃, and 2 CaCl₂; bubbled with 95% O₂/5% CO₂ (pH 7.4). Coronal hypothalamic slices (250 μ m thick) containing PVN were obtained with a VT1200 S microtome (Leica Microsystems) in cold, oxygenated aCSF. Coronal slices were then maintained for recovery for at least 45 minutes at room temperature (22°C–24°C) before the start of the electrophysiological recordings. For electrophysiological recordings, individual slices were transferred to a recording chamber (~0.5 mL of volume) and perfused with continuously bubbled (95% O₂, 5% CO₂) aCSF at a rate of 3 mL min⁻¹. The flow rate was controlled by a Perfusion Valve Control System (Warner Instruments), and recording temperature was maintained at 30°C–32°C using a Dual Channel Temperature Controller (TC-344C, Warner Instruments). Voltage-clamp recordings were made with an Axopatch 200B amplifier with Digidata (Molecular Devices). TH⁺ cells in the PVN were visualized by epifluorescence (tdTomato Reporter) using a fixed-stage upright microscope Olympus BX54WI (Olympus Corporation) equipped with a water-immersion objective (60 \times ; LUMPlan FL N, FN26.5, Olympus). Borosilicate glass (1.5 mm OD, 1.17 mm ID; BF150-117-10, P-87; Sutter Instruments) was used to prepare the recording electrodes of 2 to 4 M Ω with a horizontal puller (P-87; Sutter Instruments) and filled with aCSF solution. Assays were aborted if the series resistance was unstable throughout the recording (>20% change). Currents were low-pass filtered at 2 kHz and sampled at 10 kHz. An agar-KCl (1M) bridge was used to ground the recording chamber to the bath.

The cell-attached recordings were performed with extracellular aCSF solution. To isolate and record the SFR resulting from activation of voltage-gated cation channels, we abolished all the synaptic transmission by adding a GABA-A receptor antagonist (picrotoxin, 50 μ M), an antagonist of AMPA/kainate receptors (CNQX, 5 μ M), and an NMDA receptor antagonist (D-APV, 50 μ M), which were obtained from Sigma-Aldrich. Stock solutions of the drugs were prepared and maintained at -20°C until use: picrotoxin (50 mM in ethanol), CNQX (5 mM in DMSO), and D-APV (50 mM in water). To obtain the final concentration, the stock solution was diluted in aCSF. All recordings were obtained from tdTomato⁺ cells from the TH^{Cre}tdTomato^{fl/+} PVN slices, using a combination of fluorescence illumination (excitation [Ex] = 554, emission [Em] = 581nm) and infrared differential interference contrast (IR-DIC) microscopy. The SFR was recorded in voltage-clamp mode with 0 mV of holding potential and a loose resistance cell (<1 G Ω). The effects of prorenin (PR, 2.5 nM) (ANASPEC) and PRO20 (250 nM, ChinaPeptides) on SFR were recorded. At the end of the experiments, tetrodotoxin (1 μ M), a Na⁺ channel inhibitor, was added to the bath to abolish and confirm neural activity. Data are shown as mean \pm SEM. The SFR was analyzed with Clampfit 11.1 (Molecular Devices).

Continuous monitoring of blood pressure and heart rate by telemetry probes. Two weeks after receiving the bilateral injection of AAV2-TH-Cre into the PVNs, the PRR-tdTomato-LoxP and the tdTomato-LoxP mice were implanted with telemetry radio transmitters (PA-C10, DSI, Harvard Bioscience Inc.) to continuously monitor blood pressure, heart rate, and locomotor activity levels in awake, freely moving mice (20, 30, 60). Briefly, mice were anesthetized using 4%–5% isoflurane in 100% O₂ and flushed at 1 L/min for 2 minutes, and anesthesia was subsequently maintained using 1.5% isoflurane. The oblique and tracheal muscles were separated to expose the left carotid artery. The probe catheter was implanted into the left carotid artery and secured with a suture. The body of the radio transmitter was s.c. implanted in the right flank under the arm. Two weeks after recovery from surgery, blood pressure, heart rate, and locomotor activity were recorded continuously at baseline before HFD and following 6 weeks of HFD.

Continuous glucose monitoring and DREADD activation of PVNTH neurons. One month following the bilateral injection of either AAV2-TH-GFP (control) or AAV2-TH-Cre in the PVN of hM4Di^{fl/fl} mice as described above, mice were implanted with radiotelemetry transmitters (HD-XG, DSI, Harvard Bioscience Inc.) to continuously monitor blood glucose levels in awake, freely moving mice. Briefly, mice were anesthetized using 4%–5% isoflurane in 100% O₂ and flushed at 1 L/min for 2 minutes, and anesthesia was subsequently maintained using 1.5% isoflurane. The oblique and tracheal muscles were separated to expose the left carotid artery (19, 20, 31, 61). The glucose radio telemetry transmitter (HD-XG) catheter was implanted into the left carotid artery and secured with a suture. The body of the radio transmitter was s.c. implanted in the right flank under the arm.

Mice were allowed to recover from surgery for 1 week, and telemetry transmitters were calibrated twice a week according to the manufacturer's recommendations. Briefly, the calibrations consisted of measuring blood glucose levels using a Nova StatStrip Xpress glucometer (Nova Biomedical) initially at baseline and following an i.p. injection of glucose (2 g/Kg). After that, baseline blood glucose was measured using a test strip twice weekly. This procedure collected blood directly on a blood glucose strip following a small tail snip performed with a razor. Blood glucose values were then entered into Ponemah software (DSI, Harvard Bioscience Inc.) and associated with current values at the specific time points in which blood glucose was measured. Following transmitter's calibration, baseline blood glucose was continuously monitored, and mice were i.p. injected with either sterile 0.9% saline (vehicle) or Clozapine-N-Oxide Dihydrochloride (CNO, catalog 6329, Tocris), a water-soluble salt of CNO, at 1 mg/Kg at least 48 hours apart; blood glucose was continuously monitored.

Statistics. Data are expressed as mean ± SEM. Outliers were identified using robust regression and outlier removal (ROUT) method, coefficient $q = 1\%$ (FDR less than 1%), using GraphPad Prism Version 10 software. Data were analyzed by 2-tailed paired Student's *t* test, unpaired Student's *t* test, Mann-Whitney *U* test, or 2-way ANOVA with a mixed-effects model and Fisher's least significant difference (LSD) tests to correct for multiple comparisons, as appropriate. Statistical comparisons were performed using GraphPad Prism Version 10 software. Differences with $P < 0.05$ were considered statistically significant.

Study approval. All procedures were conducted following the NIH *Guide for the Care and Use of Laboratory Animals* (National Academies Press, 2011) and were approved by the IACUC and the Institutional Biosafety Committee at the University of Nevada, Reno. The use of AAV was approved by the Institutional Biosafety Committee at the University of Nevada, Reno.

Data availability. Values for all data points in graphs are reported in the Supporting Data Values file.

Author contributions

SP, LACS, CJW, MERM, and AJBG were involved in the experimental design, experimental procedures, data acquisition, data analysis, and manuscript writing and editing; they all contributed equally to the data collection and presentation, and thus, they are the co-first authors of the manuscript; the order of co-first authors was determined by the significance of their contributions. ASS contributed to the electrophysiological experimental design. SGC was involved in RNAScope experimental technical support. DS was involved in data analysis and discussion of the results. RNB, GJM, MWS, and YFE participated in designing experiments, discussing results, and editing the manuscript. YFE is the guarantor of this work and, as such, has full access to all the data in the study and takes responsibility for the integrity of the data and the accuracy of the data analysis.

Acknowledgments

The investigators are supported by grants from the NIH (R01DK135621, R01HL122770, R35HL155008, 1P20GM130459 to YFE; R01DK101997 and R01DK083042 to MWS; and R01DK089056 and

R01DK124238 to GJM) and the Nutrition Obesity Research Center (NORC; P30DK035816; MWS and GJM) at the University of Washington. Research reported in this publication utilized the Transgenic Animal Genotyping and Phenotyping Core and the High Spatial and Temporal Imaging Core facilities of the University of Nevada, Reno, supported by the National Institute of Neural Medical Sciences of the NIH (NHI/NIGMS 1P20GM130459), and the FSGTs were performed by the University of Washington Diabetes Research Center (DRC; P30DK017047) and the Metabolic and Cellular Phenotyping Core at the University of Washington. BioRender.com was used in the creation of Figure 2A; Figure 3A; Figure 4A; Figure 5, A and H; Figure 6A; and Figure 7I.

Address correspondence to: Yumei Feng Earley, Professor of Pharmacology and Physiology & Cell Biology, Center for Molecular and Cellular Signaling in the Cardiovascular System, University of Nevada School of Medicine, 1664 North Virginia Street, Mail-stop 0318, Reno, Nevada 89557, USA. Email: yumeifeng@med.unr.edu.

1. Galicia-Garcia U, et al. Pathophysiology of type 2 diabetes mellitus. *Int J Mol Sci.* 2020;21(17):6275.
2. Alonge KM, et al. Brain control of blood glucose levels: implications for the pathogenesis of type 2 diabetes. *Diabetologia.* 2021;64(1):5–14.
3. Mirzadeh Z, et al. Central nervous system control of glucose homeostasis: a therapeutic target for type 2 diabetes? *Annu Rev Pharmacol Toxicol.* 2022;62:55–84.
4. Meek TH, et al. Functional identification of a neurocircuit regulating blood glucose. *Proc Natl Acad Sci U S A.* 2016;113(14):E2073–E2082.
5. Flak JN, et al. Ventromedial hypothalamic nucleus neuronal subset regulates blood glucose independently of insulin. *J Clin Invest.* 2020;130(6):2943–2952.
6. Deem JD, et al. Identification of hypothalamic glucoregulatory neurons that sense and respond to changes in glycemia. *Diabetes.* 2023;72(9):1207–1213.
7. Papazoglou I, et al. A distinct hypothalamus-to- β cell circuit modulates insulin secretion. *Cell Metab.* 2022;34(2):285–298.
8. Herrera Moro Chao D, et al. Hypothalamic astrocytes control systemic glucose metabolism and energy balance. *Cell Metab.* 2022;34(10):1532–1547.
9. Ma Y, et al. Glucose in the hypothalamic paraventricular nucleus regulates GLP-1 release. *JCI Insight.* 2020;5(8):132760.
10. Negishi K, et al. Distributions of hypothalamic neuron populations coexpressing tyrosine hydroxylase and the vesicular GABA transporter in the mouse. *J Comp Neurol.* 2020;528(11):1833–1855.
11. Shi YC, et al. Arcuate NPY controls sympathetic output and BAT function via a relay of tyrosine hydroxylase neurons in the PVN. *Cell Metab.* 2013;17(2):236–248.
12. De Kloet AD, et al. The renin angiotensin system and the metabolic syndrome. *Physiol Behav.* 2010;100(5):525–534.
13. Carine M, et al. Cassis. Activation of the systemic and adipose renin-angiotensin system in rats with diet-induced obesity and hypertension. *Am J Physiol Regul Integr Comp Physiol.* 2004;287(4):R943–R949.
14. Clafin KE, Grobe JL. Control of energy balance by the brain renin-angiotensin system. *Curr Hypertens Rep.* 2015;17(5):38.
15. Sapouckey SA, et al. Potential mechanisms of hypothalamic renin-angiotensin system activation by leptin and DOCA-salt for the control of resting metabolism. *Physiol Genomics.* 0087;49(12):722–732.
16. Xu Q, et al. The critical role of the central nervous system (pro)renin receptor in regulating systemic blood pressure. *Pharmacol Ther.* 2016;164:126–134.
17. Souza LAC, Earley YF. (Pro)renin receptor and blood pressure regulation: a focus on the central nervous system. *Curr Hypertens Rev.* 2022;18(2):101–116.
18. Nguyen G, et al. Pivotal role of the renin/prorenin receptor in angiotensin II production and cellular responses to renin. *J Clin Invest.* 2002;109(11):1417–1427.
19. Li W, et al. Intracerebroventricular infusion of the (Pro)renin receptor antagonist PRO20 attenuates deoxycorticosterone acetate-salt-induced hypertension. *Hypertension.* 2015;65(2):352–361.
20. Li W, et al. Neuron-specific (pro)renin receptor knockout prevents the development of salt-sensitive hypertension. *Hypertension.* 2014;63(2):316–323.
21. Christlieb AR, et al. Plasma renin activity and hypertension in diabetes mellitus. *Diabetes.* 1976;25(10):969–974.
22. Fernandez-Cruz A Jr. Low plasma renin activity in normotensive patients with diabetes mellitus: relationship to neuropathy. *Hypertension.* 1981;3(1):87–92.
23. Franken AA, et al. High plasma prorenin in indiathe diabetes mellitus and its correlation with some complications. *J Clin Endocrinol Metab.* 1990;71(4):1008–1015.
24. Bryer-Ash M, et al. Plasma renin and prorenin (inactive renin) in diabetes mellitus: effects of intravenous furosemide. *J Clin Endocrinol Metab.* 1988;66(2):454–458.
25. Bryer-Ash M, et al. Increased inactive renin in diabetes mellitus without evidence of nephropathy. *J Clin Endocrinol Metab.* 1983;56(3):557–561.
26. Luetscher JA, et al. Increased plasma inactive renin in diabetes mellitus. A marker of microvascular complications. *N Engl J Med.* 1985;312(22):1412–1417.
27. Stankovic AR, et al. Prorenin and angiotensin-dependent renal vasoconstriction in type 1 and type 2 diabetes. *J Am Soc Nephrol.* 2006;17(12):3293–3299.
28. Kang JJ, et al. The collecting duct is the major source of prorenin in diabetes. *Hypertension.* 2008;51(6):1597–1604.

29. Worker CJ, et al. The neuronal (pro)renin receptor and astrocyte inflammation in the central regulation of blood pressure and blood glucose in mice fed a high-fat diet. *Am J Physiol Endocrinol Metab.* 2020;318(5):E765–E778.
30. Li W, et al. Brain-targeted (pro)renin receptor knockdown attenuates angiotensin II-dependent hypertension. *Hypertension.* 2012;59(6):1188–1194.
31. Souza LAC, et al. (Pro)renin receptor knockdown in the paraventricular nucleus of the hypothalamus attenuates hypertension development and AT₁ receptor-mediated calcium events. *Am J Physiol Heart Circ Physiol.* 2019;316(6):H1389–H1405.
32. Pitra S, et al. Exacerbated effects of prorenin on hypothalamic magnocellular neuronal activity and vasopressin plasma levels during salt-sensitive hypertension. *Am J Physiol Heart Circ Physiol.* 2019;317(3):H496–H504.
33. Pitra S, et al. Mechanisms underlying prorenin actions on hypothalamic neurons implicated in cardiometabolic control. *Mol Metab.* 2016;5(10):858–868.
34. Cooper SG, et al. Renin-a in the subfornical organ plays a critical role in the maintenance of salt-sensitive hypertension. *Biomolecules.* 2022;12(9):1169.
35. Alonso LC, et al. Simultaneous measurement of insulin sensitivity, insulin secretion, and the disposition index in conscious unhandled mice. *Obesity (Silver Spring).* 2012;20(7):1403–1412.
36. Sharabi K, et al. Molecular pathophysiology of hepatic glucose production. *Mol Aspects Med.* 2015;46:21–33.
37. Ramnanan CJ, et al. Physiologic action of glucagon on liver glucose metabolism. *Diabetes Obes Metab.* 2011;13 Suppl 1(suppl 1):118–125.
38. Morton GJ, et al. FGF19 action in the brain induces insulin-independent glucose lowering. *J Clin Invest.* 2013;123(11):4799–4808.
39. Scarlett JM, et al. Central injection of fibroblast growth factor 1 induces sustained remission of diabetic hyperglycemia in rodents. *Nat Med.* 2016;22(7):800–806.
40. Yin W, Gore AC. The hypothalamic median eminence and its role in reproductive aging. *Ann N Y Acad Sci.* 2010;1204:113–122.
41. Hyun U, Sohn JW. Autonomic control of energy balance and glucose homeostasis. *Exp Mol Med.* 2022;54(4):370–376.
42. Myers MG, et al. Central nervous system regulation of organismal energy and glucose homeostasis. *Nat Metab.* 2021;3(6):737–750.
43. Hardy SG. Hypothalamic projections to cardiovascular centers of the medulla. *Brain Res.* 2001;894(2):233–240.
44. O'Hare JD, Zsombok A. Brain-liver connections: role of the preautonomic PVN neurons. *Am J Physiol Endocrinol Metab.* 2016;310(3):E183–E189.
45. Geerling JC, et al. Paraventricular hypothalamic nucleus: axonal projections to the brainstem. *J Comp Neurol.* 2010;518(9):1460–1499.
46. Pan S, et al. The hypothalamus as a key regulator of glucose homeostasis: emerging roles of the brain renin-angiotensin system. *Am J Physiol Cell Physiol.* 2023;325(1):C141–C154.
47. Sakoda M, et al. (Pro)renin receptor-mediated activation of mitogen-activated protein kinases in human vascular smooth muscle cells. *Hypertens Res.* 2007;30(11):1139–1146.
48. Son SJ, et al. Dendritic peptide release mediates interpopulation crosstalk between neurosecretory and preautonomic networks. *Neuron.* 2013;78(6):1036–1049.
49. Rotondo F, et al. Arginine vasopressin (AVP): a review of its historical perspectives, current research and multifunctional role in the hypothalamo-hypophysial system. *Pituitary.* 2016;19(4):345–355.
50. De Kloet AD, et al. Central angiotensin II has catabolic action at white and brown adipose tissue. *Am J Physiol Endocrinol Metab.* 2011;301(6):E1081–E1091.
51. Porter JP, Potratz KR. Effect of intracerebroventricular angiotensin II on body weight and food intake in adult rats. *Am J Physiol Regul Integr Comp Physiol.* 2004;287(2):R422–R428.
52. Claflin KE, et al. Angiotensin AT1A receptors on leptin receptor-expressing cells control resting metabolism. *J Clin Invest.* 2017;127(4):1414–1424.
53. Meek TH, et al. BDNF action in the brain attenuates diabetic hyperglycemia via insulin-independent inhibition of hepatic glucose production. *Diabetes.* 2013;62(5):1512–1518.
54. Daigle TL, et al. A suite of transgenic driver and reporter mouse lines with enhanced brain-cell-type targeting and functionality. *Cell.* 2018;174(2):465–480.
55. Savitt JM, et al. Bcl-x is required for proper development of the mouse substantia nigra. *J Neurosci.* 2005;25(29):6721–6728.
56. Madisen L, et al. A robust and high-throughput Cre reporting and characterization system for the whole mouse brain. *Nat Neurosci.* 2010;13(1):133–140.
57. Zhu H, et al. Cre-dependent DREADD (designer receptors exclusively activated by designer drugs) mice. *Genesis.* 2016;54(8):439–446.
58. De Kloet AD, et al. Reporter mouse strain provides a novel look at angiotensin type-2 receptor distribution in the central nervous system. *Brain Struct Funct.* 2016;221(2):891–912.
59. Bergman RN, et al. Quantitative estimation of insulin sensitivity. *Am J Physiol.* 1979;236(6):E667–E677.
60. Peng H, et al. Overexpression of the neuronal human (pro)renin receptor mediates angiotensin II-independent blood pressure regulation in the central nervous system. *Am J Physiol Heart Circ Physiol.* 2018;314(3):H580–H592.
61. Souza LA, et al. Use of chlorisondamine to assess the neurogenic contribution to blood pressure in mice: an evaluation of method. *Physiol Rep.* 2021;9(3):e14753.